Conformational Dynamics of Trialanine in Water. 2. Comparison of AMBER, CHARMM, GROMOS, and OPLS Force Fields to NMR and Infrared Experiments

Yuguang Mu, Daniil S. Kosov, and Gerhard Stock*

Institute of Physical and Theoretical Chemistry, J. W. Goethe University, Marie-Curie-Str. 11, D-60439 Frankfurt, Germany

Received: November 14, 2002; In Final Form: January 17, 2003

Driven by recent two-dimensional infrared experiments by Woutersen and Hamm, trialanine has emerged as a paradigm to study conformational dynamics of a small peptide in aqueous solution. Employing the exceptional amount of experimental and ab initio data, in this work, trialanine serves as a model problem to perform a comprehensive comparison of six popular force fields, including the recent versions of the AMBER, CHARMM, GROMOS, and OPLS models. For all force fields under consideration, 20 ns long molecular-dynamics simulations are performed, and the structure and conformational dynamics of the solvated peptide is studied in detail. Employing density-functional theory calculations at the B3LYP/6-31+G(d) level, a number of observable quantities are calculated directly from the molecular-dynamics data and compared to experiment. The comparison allows for a quite detailed interpretation of recent NMR and infrared experiments. The nowadays achievable reliability and accuracy of a molecular dynamics description of a highly flexible biomolecular system are discussed in some detail.

1. Introduction

Classical molecular dynamics (MD) simulations have become a powerful tool to study the structure, dynamics, and function of complex molecular systems in atomic detail.[1−7] The quality of a MD calculation depends on (i) the validity of the underlying classical approximation, (ii) whether the sampling of phase space is sufficient for the system properties under consideration, and (iii) the accuracy of the force field employed, that is, the empirical potential-energy functions defining the interactions between the atoms. To be able to treat complex biomolecular systems such as proteins and nuclear acids, commonly used force fields need to find a compromise between accuracy and computational efficiency. To this end, usually only two-body interactions are considered, polarization effects are neglected, and a simple functional form of the potential-energy function is assumed. Remarkably, this approach has been shown to reproduce experimentally determined equilibrium structures in many cases. Only little is known, however, about the reliability of a force-field description of dynamical processes such as conformational transitions or the folding of biomolecules.

To investigate dynamical properties of proteins, it is instructive to consider small peptides which mimic building blocks of the actual polypeptide backbone. This is because, contrary to larger molecules whose secondary structures are stabilized by intramolecular hydrogen bonds, these small systems may exhibit fast conformational transitions, which can be studied under equilibrium conditions. Experimentally, reliable data on the conformations of peptide building blocks has become available very recently with the advent of two-dimensional (2D) infrared (IR) spectroscopy.[8−13] Although the physical background of this method is similar to 2D nuclear magnetism resonance (NMR) techniques,[14] the time scale of IR experiments of ≈1 ps is sufficiently fast to resolve the dynamics in individual conformational states. On the theoretical side, di- and tripeptides are sufficiently small to allow for high-level ab initio and density-functional theory (DFT) methods.[7,15−21] Because MD simulations including explicit solvent are nowadays readily performed on a 10 ns time scale, moreover, for small peptides, there is virtually no sampling problem for most observables of interest.[21−32]

Recently, a number of experimental studies have been reported for trialanine, a small peptide with two peptide bonds and one set of dihedral angles (ϕ,ψ).[11−13,33−37] Woutersen and Hamm have presented various 2D-IR studies, which suggested that trialanine mostly adopts a conformation around $(\phi,\psi) \approx (-60°, +140°)$, known as poly(Gly)II ($P_{II}$) structure.[11−13] This finding was confirmed by NMR investigations[33−35] as well as by polarized Raman and FTIR experiments.[36] Very recently, however, new experimental data have suggested that trialanine may also exist to a smaller amount in the right-handed helix conformation α_R located at $\approx(-80°, -50°)$ and in the extended conformation β located at $\approx(-120°, +130°)$. The observation of a significant inhomogeneity of the nonlinear-IR spectrum was interpreted as a consequence of transitions between the P_{II} and the α_R conformations.[35] The evidence for a β conformation comes from an extended polarized Raman and FTIR study.[37]

The discussion above reflects the notorious problem of interpreting spectroscopic experiments in the condensed phase. Although these experiments provide a wealth of data, their interpretation usually relies on highly simplified models and assumptions, which often hamper clear and unambiguous conclusions. From a theoretician's point of view, one would therefore like to pursue an independent and unbiased theoretical description and *directly* calculate the experimental data such as IR intensities, cross relaxation rates, and NMR couplings from a combined MD/quantum-chemical approach. With this end in mind, we have recently performed a 20 ns MD simulations of trialanine using the *GROMOS96* force-field (paper 1[31]). The calculations predicted that solvated trialanine

* To whom correspondence should be addressed. E-mail: stock@theochem.uni-frankfurt.de.

10.1021/jp022445a CCC: $25.00
Published on Web 05/02/2003

is predominantly found in the extended conformations β (≈40%) and P_{II} (≈40%) and also (≈16%) in the helix conformation α_R. Furthermore, we have performed extensive DFT calculations on isolated trialanine on the B3LYP/6-31+G(d) level of theory, thus generating two-dimensional frequency maps $\omega(\phi,\psi)$ of the vibrational modes of trialanine.[38] Employing these maps and related ab initio data by Torii and Tasumi,[39] we have evaluated the 20 ns MD trajectory of trialanine to compute a number of measurable data, including the mean amid I cross-coupling, the cross-relaxation correlation function, and the resulting cross-relaxation rates, as well as the frequency-fluctuation correlation function and the resulting line width broadening.[35,31] We note that the MD/DFT approach to the calculation of experimental observables outlined above should not be confused with a "QM/MM" description, in which the potential energy is calculated in a mixed quantum-mechanical (QM) and molecular-mechanics (MM) force field.

Although the theoretical results are in good overall agreement with available experimental data, there still remains a considerable uncertainty in the interpretation of the results. This is because the relative population probabilities of the various conformations are determined by the Boltzmann factor $\exp(-\Delta G/k_BT)$, where $\Delta G/k_BT$ may be quite small for biophysical systems. To make reliable predictions of the populated conformations of the peptide, therefore, an accuracy of ΔG of less than $k_BT = 2.5$ kJ/mol is required, which clearly represents a great challenge for an empirical force field. As the accuracy of the potential-energy models appears to be the bottleneck of the theoretical description, it seems worthwhile to investigate the quality of various force fields in some detail.[40] Given the exceptional amount of experimental and ab initio data, trialanine appears to be an excellent model problem for this purpose.

In this work, we are concerned with a comprehensive comparison of six different force fields that have been widely used for peptides and proteins. In a first step, the gas-phase energies of the various force fields are compared to high-level ab initio data, and general trends of the models are discussed. Then for each force field, a 20 ns MD simulation is performed. We analyze the contributions of intra- and intermolecular interactions as well as the entropic contributions to the free energies of the stable conformers. When the results of the MD and DFT calculations are combined, a number of measurable quantities are calculated and compared to available experimental data. The comparison allows for a quite detailed interpretation of the experiments. Although a case study on a specific peptide cannot assess the overall behavior of a general biomolecular force field, nevertheless, it indicates the nowadays achievable reliability and accuracy of a MD description of a highly flexible biomolecular system.

2. Computational Methods

2.1. Force Fields. Most force fields for biomolecular simulations are described by an empirical potential-energy expression of the form

$$V = \sum_{\text{bonds}} K_r(r - r_{\text{eq}})^2 + \sum_{\text{angles}} K_\theta(\theta - \theta_{\text{eq}})^2 + \sum_{\text{dihedrals}} \frac{V_n}{2}[1 + \cos(n\phi - \delta_n)] + \sum_{i<j}\left[\frac{A_{ij}}{R_{ij}^{12}} - \frac{R_{ij}}{R_{ij}^{6}} + \frac{q_i q_j}{\epsilon R_{ij}}\right] \quad (1)$$

Here, the first three terms comprise the intramolecular or bonded interactions, where the bonds and angles are represented by a simple harmonic expression and the dihedral energies are modeled by a Fourier expansion. The double sum accounts for the intermolecular or nonbonded interactions, where the van der Waals interaction is treated by a 6−12 potential and the electrostatic interactions are modeled by a Coulomb potential of atom-centered point charges. The nonbonded interactions are only considered between atoms in different molecules or for atoms of the same molecules separated by at least three bonds. Nonbonded interactions separated by exactly three bonds are usually reduced by a scale factor ("1−4 interactions"). Although the general form of the potential-energy function is similar for most biomolecular force fields, the various models differ significantly in their parametrization; that is, the strategy the potential-energy parameters are derived from experimental and ab initio data. For a discussion of the various philosophies in force-field development, see, for example, refs 41−47.

For the MD simulations of trialanine, we have employed six different force fields which throughout the paper are discussed in alphabetical order. A widely used force field is the parm94.dat version of AMBER,[41] henceforth referred to as A94. We also considered the parm96 (A96) version of AMBER,[42] that differs from A94 in the parametrization of the dihedral parameters. A second well-known potential-energy model is the version 22 of the CHARMM force field,[43] which was published in 1998 and is referred to as C98. Of the GROMOS96 simulation package,[44] two parameter sets were considered, the standard set 43A1 (G96) and a refined set 45A3 (G01) published recently.[45] Finally, we considered the all-atom version of the OPLS force field,[46] which is referred to as O96.

2.2. MD Simulations. Three MD program packages were used in this work, that is, AMBER 6 [48] for the AMBER and OPLS force fields, CHARMM[43] for the CHARMM force field, and GROMOS96[44] for the GROMOS force fields. Because of the large similarity of the OPLS and AMBER force fields, the O96 parameters could be readily implemented into the AMBER 6 program.

In all simulations using the AMBER 6 and the CHARMM programs, trialanine was placed in a periodic cubic box of TIP3 water.[49] A minimum solute-to-wall distance of 1 nm was used, giving a box length of 3.3 nm and containing ≈1150 water molecules. Assuming that the terminal groups are fully protonated to account for the experimental situation of pH = 1,[11] the all-atom description of trialanine consists of 34 atoms. The equation of motion was integrated by using a leapfrog algorithm with a time step of 2 fs. Covalent bond lengths were constrained by the SHAKE algorithm with a relative geometric tolerance of 0.0001.[50] A cutoff of 1.0 nm was used for the nonbonded interactions. The nonbonded interaction pair-list was updated every 20 fs. The solute and solvent were separately weakly coupled to external temperature baths at 300 K.[51] The temperature coupling constant was 0.1 ps (0.01 during the first 10 ps). The total system was also weakly coupled to an external pressure bath at 1 atm using a coupling constant of 0.5 ps (0.05 during the first 10 ps).

The united-atom force fields G96 and G01 were run in the GROMOS96 program package. Here, trialanine was placed in a periodic truncated octahedral box of simple point charge (SPC) water.[52] A minimum solute-to-wall distance of 1.35 nm was used, giving a box length of 4.04 nm and a total 1083 water molecules. A twin-range cutoff of 0.8/1.4 nm was used for the nonbonded interactions, and a reaction-field correction with permittivity $\epsilon_{RF} = 54$ was employed.[5] All other details of the simulation were as described above for the AMBER 6 program.

Starting with a fully extended configuration of trialanine, the equilibration protocol for all simulations consisted of 100 steps

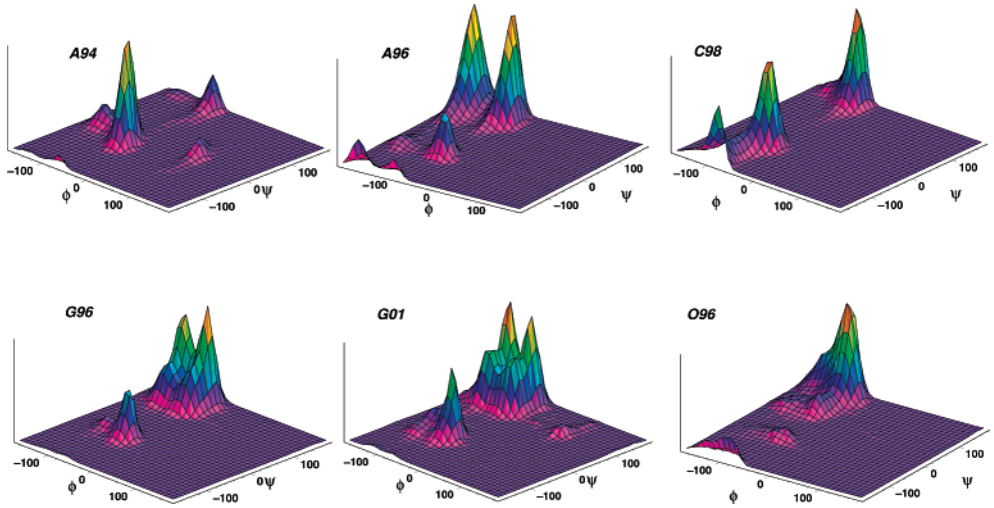

Figure 1. Ramachandran ϕ,ψ probability distribution of trialanine in water as obtained from 20 ns MD simulations employing various force fields.

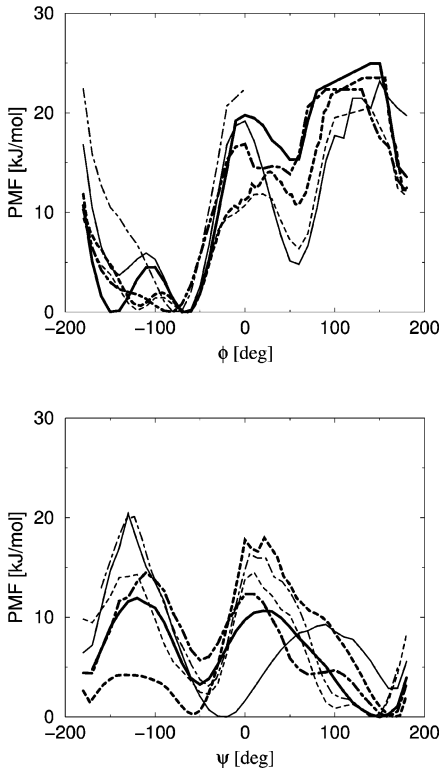

Figure 2. Potentials of mean force along the central dihedral angles ϕ and ψ, obtained from unbiased MD simulations using the force fields A94 (thin solid lines), A96 (thick solid lines), C98 (thin dotted-dashed lines), G96 (thick dashed lines), G01 (thin dashed lines), and O96 (thick dotted-dashed lines).

of steepest-descent minimization applied to the solvent molecules with fixed solute, followed by 5 ps of MD simulation at 300 K of the solvent with fixed trialanine, and another 5 ps simulation without position constraining of trialanine. The simulations were then continued for 20 ns, and the coordinates were recorded every 0.1 ps for analysis.

In addition to the simulations presented below, we have performed numerous test calculations to ensure the significance and convergence of our studies. Concerning the appropriate treatment of the electrostatic interactions, we have checked the invariance of our results with respect to (i) an increase of the cutoffs, (ii) the usage of the Ewald method, and (iii) the inclusion of a counterion. To ensure the quality of the sampling, we have (i) compared the ϕ,ψ free-energy profiles in Figure 2 to independent umbrella-sampling calculations,[53] (ii) performed several long simulations at $T = 350$ K, and (iii) performed a number of simulation with various initial conditions, acquiring a total simulation time of about 500 ns. See the Supporting Information.

2.3. Calculation of Free Energy and Entropy. One-dimensional potentials of mean force along the central dihedral angles ϕ and ψ were calculated directly from the unbiased MD simulation described above. The probability distribution $P(\phi)$ was obtained from a histogram of the MD data for $\phi(t)$ using a step size of 8°. The free-energy profile along ϕ is then given by

$$\Delta G(\phi) = -k_B T[\ln P(\phi) - \ln P_{max}] \qquad (2)$$

where P_{max} denotes the maximum of the distribution $P(\phi)$, which is subtracted to ensure that $\Delta G = 0$ for the lowest free-energy minimum. The same procedure was performed to obtain $\Delta G(\psi)$.

To investigate the origin of the free-energy difference ΔG, the thermodynamic relation

$$\Delta G = \Delta H - T\Delta S \qquad (3)$$

was employed. Here, the changes in the enthalpy ΔH of trialanine are readily calculated from the potential energies of the system. To calculate the entropic contribution to the free energy, a principal component analysis of the atom-positional fluctuations of trialanine was performed.[54,55] Assuming that the fluctuations observed in the MD simulation can be described by a multivariate Gaussian probability distribution, the principal component analysis maps the system on an ensemble of independent harmonic oscillators, the entropy of which is given by

$$S = k_B \sum_{i=1} \frac{\hbar\omega_i/k_B T}{e^{\hbar\omega_i/k_B T} - 1} - \ln(1 - e^{\hbar\omega_i/k_B T}) \qquad (4)$$

For the technical details of the entropy calculations, see paper 1.[31]

3. Results and Discussion

3.1. Gas-Phase Calculations. It is instructive to first consider the quality of the various force fields by a direct comparison to ab initio calculations. As mentioned in the Introduction, we have

performed extensive DFT studies of isolated trialanine,[38] which in the following will be used as a reference. All calculations were performed using Gaussian 98[56] at the B3LYP/6-31+G(d) level of theory, which was found to yield very good overall agreement with MP2 data. Although it is understood that the B3LYP/6-31+G(d) results cannot be regarded as quantitatively correct for total energies,[57] they nevertheless may provide a valuable overall description of the conformational energies of the system.

To characterize the potential energy of trialanine as a function of the central dihedral angles ϕ and ψ, we have performed restricted geometry optimizations with fixed ϕ and ψ. To cover the extended (β and P_{II}) and the helix (α_R) regions as well as the transition states between these conformations, we have calculated about 200 points which are nearly equally distributed in the Ramachandran space defined by $-150° \le \phi \le -20°$ and $-60° \le \psi \le +150°$. The trialanine geometries obtained from the DFT calculations were then used as starting geometries for the subsequent force-field calculations. In the course of the molecular-mechanics geometry optimizations, all dihedral angles were constrained to the corresponding ab initio values. As is well-known,[7,15-20] both force-field and DFT calculations of isolated di- and tripeptides predict that the β state represents the conformation of lowest energy.

To obtain an overall picture of the conformational energies, we have averaged the energy deviations $\delta E = E^{FF} - E^{DFT}$ between the force-field and DFT results over $N = 21$ representative (ϕ,ψ) geometries of the helix (α_R) and extended (β/P_{II}) conformations, i.e., we have calculated

$$\langle \delta E_\alpha \rangle = \frac{1}{N} \sum_{n=1}^{N} (E_{\alpha n}^{FF} - E_{\alpha n}^{DFT}) \quad (5)$$

$$\langle \delta E_{\beta P_{II}} \rangle = \frac{1}{N} \sum_{n=1}^{N} (E_{\beta P_{II} n}^{FF} - E_{\beta P_{II} n}^{DFT}) \quad (6)$$

In particular, it is instructive to consider the difference of these deviations

$$E_{\alpha,\beta P_{II}} \equiv \langle \delta E_\alpha \rangle - \langle \delta E_{\beta P_{II}} \rangle \quad (7)$$

which indicates whether a given force field favors the helix state ($E_{\alpha,\beta P_{II}} < 0$) or the extended states ($E_{\alpha,\beta P_{II}} > 0$). We also considered the root-mean-square (RMS) deviations

$$\delta E_j^2 = \frac{1}{N_j} \sum_{n_j=1}^{N_j} (E_{n_j}^{FF} - E_{n_j}^{DFT} - E_j^0)^2 \quad (8)$$

with $j = \beta/P_{II}$ for the extended conformations, $j = \alpha$ for the helix conformation, and $j =$ all for the average over all conformations. For every force field and conformation, the overall energy shift E_j^0 was determined by minimizing the corresponding RMS deviation δE_j^2.

Table 1 lists the RMS deviations and the deviation difference of the conformational energies obtained for the force fields under consideration. The overall RMS deviation δE_{all}^2 is seen to range between 3 and 7 kJ/mol, which appears to be a reasonable accuracy for this kind of comparison. It is noted that all force fields (except for C98) show larger RMS deviations for the helix geometries than for the extended geometries. Considering the mean deviation difference $E_{\alpha,\beta P_{II}}$, we find the interesting trend that the force fields A94 and C98 favor the helix conformation, whereas the force fields A96, G96, G01, and O96 favor the extended conformations. Here, the large deviations of the GROMOS force fields may reflect the fact that these models are exclusively designed for condensed-phase simulations.[58] In agreement with previous MP2 calculations of Friesner and coworkers,[17,20] we note a good overall performance of the OPLS force field. This is even more the case for the lastest version of the OPLS model,[19] which was refitted to high-level ab initio calculations.

TABLE 1: Gas-Phase Conformational Energies of Trialanine, Comparing DFT (B3LYP/6-31+G(d)) and Force-Field Calculations[a]

model	$\delta E_{\alpha,\beta P_{II}}$	$\delta E_{\beta P_{II}}^2$	δE_α^2	δE_{all}^2
A94	−8.28	2.50	3.84	5.28
A96	3.29	1.40	4.98	4.77
C98	−4.23	5.78	3.29	5.05
G96	7.80	4.29	5.91	6.58
G01	10.51	4.97	6.07	7.51
O96	2.49	2.64	2.59	3.22

[a] Shown are the mean deviation difference $\delta E_{\alpha,\beta P_{II}}$ [eq 7] and the RMS deviations δE^2 [eq 8] for the extended (β/P_{II}) and helical (α) conformers. All units are kJ/mol.

TABLE 2: Conformations of Trialanine Sampled during the 20 ns MD Simulations Using Various Force Fields[a]

model	state	ϕ [deg]	ψ [deg]	$\Delta\phi$ [deg]	$\Delta\psi$ [deg]	P [%]
A94	β	−139	162	14	22	5
	P_{II}	−68	159	13	20	22
	α_R	−79	−26	28	21	71
	α_L	56	9	12	31	2
A96	β	−144	140	14	37	44
	P_{II}	−69	140	14	26	41
	α_R	−97	−49	40	21	14
C98	β/P_{II}	−93	167	22	26	55
	α_R	−89	−71	19	26	45
G96	β	−122	130	17	24	42
	P_{II}	−67	132	15	22	41
	α_R	−76	−44	27	15	16
	α_L	41	86	23	69	1
G01	β	−125	124	18	28	41
	P_{II}	−69	128	15	25	34
	α_R	−82	−50	29	18	22
	α_L	53	100	16	40	3
O96	β/P_{II}	−102	137	35	39	88
	α_R	−90	−41	34	22	12

[a] For each conformer, the average dihedral angles ϕ and ψ, the corresponding RMS deviations $\Delta\phi$ and $\Delta\psi$, and the population probability P are given.

3.2. Conformational States and Free Energies. The remainder of the paper is concerned with the dynamics of trialanine in aqueous solution. To get a first impression of the performance of the various force fields, Figure 1 shows a Ramachandran representation of the probability distribution for the central dihedral angles (ϕ,ψ). As may be expected, there are essentially three conformational states populated, the right-handed helix conformation α_R located at $(\phi,\psi) \approx (-80°, -50°)$ and two extended conformations β ($-120°$, $+130°$) and P_{II} ($-70°$, $+130°$). A stereoview of the three conformers is given in paper 1.[31] Moreover, two force fields (A94) and (G01) show a small population of the left-handed helix conformation α_L ($+53°$, $-100°$). For all simulations, the average values for (ϕ,ψ), their RMS deviations, as well as the population probability of each conformer are listed in Table 2.

At first sight, the (ϕ,ψ) distributions of the various force fields appear to be surprisingly different. A closer inspection reveals, however, that the force fields AMBER A96, GROMOS G96 and G01, and OPLS O96 are quite similar in that they predict that solvated trialanine is predominantly (≈80%) found in the

TABLE 3: Contributions to the Free-Energies of the Helix (α_R) and the Extended (β, P_{II}) Configurations[a]

model	state	V^S_{bond}	V^S_{vdW}	V^S_{el}		$V^{SB}_{vdW}V^{SB}_{el}$	V_{tot}	$-TS$	ΔG_{tot}	$\Delta G_{\alpha\beta}$
A94	α_R	118.2	4.4	−167.9	−50.5	−683.8	−779.5	−182.0	−961.5	
	β/P_{II}	122.5	7.9	−183.0	−52.7	−641.7	−747.0	−208.0	−955.0	
	Δ	−4.3	−3.5	15.1	2.2	−42.1	−32.5	26.0	−6.5	−2.5
A96	α_R	124.7	5.17	−84.4	−6.4	−989.8	−950.7	−174.0	−1124.7	
	β/P_{II}	120.0	7.7	−115.0	−8.6	−933.2	−929.1	−196.1	−1125.2	
	Δ	4.8	−2.6	30.6	2.2	−56.6	−21.6	22.1	0.5	4.5
C98	α_R	133.8	−3.3	183.3	−54.2	−684.1	−424.5	−142.1	−566.6	
	β/P_{II}	133.0	−1.5	164.2	−52.0	−652.8	−409.1	−150.2	−559.3	
	Δ	0.8	−1.8	19.1	−2.2	−31.3	−15.4	8.1	−7.3	0.5
G96	α_R	50.2	−15.6	−20.9	−39.6	−582.1	−607.8	−132.2	−740.0	
	β/P_{II}	49.1	−14.7	−42.9	−41.3	−546.0	−595.8	−141.6	−737.4	
	Δ	1.1	−0.9	22.0	1.7	−36.1	−12.0	9.4	−2.6	4.0
G01	α_R	50.9	−20.8	−21.1	−35.6	−562.2	−588.1	−147.8	−735.9	
	β/P_{II}	49.9	−19.7	−40.5	−37.9	−528.1	−576.3	−156.9	−733.2	
	Δ	1.0	−0.4	19.3	2.3	−34.0	−11.7	9.1	−2.7	3.1
O96	α_R	157.5	18.1	−298.0	13.6	−1033.8	−1142.6	−179.6	−1322.2	
	β/P_{II}	150.3	20.9	−322.0	11.8	−991.7	−1130.4	−193.1	−1323.5	
	Δ	7.2	−2.8	24.0	1.8	−42.2	−12.2	13.5	1.3	5.0

[a] Listed are the averages of the potential energies pertaining to the solute (superscript S), the solute−solvent interactions (superscript *SB*), and the entropic contribution to the free energy at $T = 300$ K. The resulting total free-energy difference ΔG_{tot} is compared to the true free-energy difference $\Delta G_{\alpha\beta}$ as obtained from the population probabilities of the conformers. All energies are given in kJ/mol.

extended conformations β and P_{II} and only little (≈20%) in the helix conformation α_R. The four models differ mainly in the free-energy barrier between the two extended conformations β and P_{II}; that is, the two states are completely separated in A96, partially in G96 and G01, and not at all in O96. On the other hand, the AMBER A94 and the CHARMM C98 force fields predict a large population of the helical α_R conformation, whereas β conformer is not populated at all. This finding is in agreement with previous MD studies on alanine dipeptide ($CH_3CO-Ala-NHCH_3$), which also showed that the force fields A94 and C98 preferably populate the α_R conformation.[28]

It is instructive to consider the relative free energies associated with the various conformations. Figure 2 shows the potentials of mean force in the coordinates ϕ and ψ as obtained from eq 2. The potentials in ϕ exhibit three minima at ≈ −120°, −70°, and +50°, which correspond to the β, P_{II}/α_R, and α_L conformers, respectively. Although the barrier between the two extended structures is shallow to nonexistent, there is a significant barrier (≈20 kJ/mol) to approach the left-handed α_L conformation. The potential of mean force in ψ describes the transition between the helix conformation α_R (≈ −50°) and the extended conformations β and P_{II} (≈160°). Interestingly, the free-energy difference between the two conformers is seen to depend significantly on the force field under consideration.

To investigate the origin of the free-energy difference between the helix and the extended conformations, the changes of enthalpy and entropy were evaluated and comprised in Table 3. The enthalpic contributions was obtained by averaging the solute−solute interaction energies V^S and the solute−solvent interaction energies V^{SB} separately for the helix and extended conformations. As listed in Table 3, the covalently bonded interaction energies V^S_{bond} as well as the nonbonded van der Waals energies V^S_{vdW} and V^{SB}_{vdW} differ only little for the two types of conformers. The main contribution to ΔH stems from the electrostatic interaction energies V^S_{el} and V^{SB}_{el}. Because of their large dipole moments, the α_R conformers show a strong electrostatic interaction with the polar water molecules and are therefore favored in energy by about $\Delta V^{SB}_{el} = 30-50$ kJ/mol. This energy gain is partly compensated by the solute−solute electrostatic interactions around $\Delta V^S_{el} = 15-30$ kJ/mol, which reflect the strong Coulomb repulsions associated with the compact helix conformations.

The entropic contribution [eq 4] to the free-energy difference, on the other hand, is found to favor the extended conformations over the helix conformations by 10−20 kJ/mol. This finding is explained by the fact that the internal motion of an interconnected helix is more restricted than the internal motion of an extended conformation. By adding the enthalpic (ΔV_{tot}) and the entropic ($-T\Delta S$) contributions, the total free-energy difference ΔG_{tot} between the helix and the extended conformations varies between −7 and +1 kJ/mol. This result is in variance with the true free-energy difference $\Delta G_{\alpha\beta}$ as obtained from the population probabilities of the conformers. The comparison therefore indicates a significant (4−8 kJ/mol) contribution of the solvent ΔG_{solv} to the free-energy difference; that is, we obtain

$$\Delta G_{\alpha\beta} = \Delta V_{tot} - T\Delta S + \Delta G_{solv} \tag{9}$$

Because $\Delta G_{solv} > 0$, the solvent contribution favors the extended conformations, which indicates that ΔG_{solv} is of entropic origin. Although the overall free-energy difference $\Delta G_{\alpha\beta}$ is relatively similar (between −2 and +5 kJ/mol) for all force fields under consideration, the individual contributions to $\Delta G_{\alpha\beta}$ are found to depend on the specific model. For example, the force fields C98, G96, G01, and O96 exhibit similar enthalpies ($\Delta V_{tot} \approx -12$ kJ/mol) and entropies ($-T\Delta S \approx -10$ kJ/mol), but the AMBER force fields A94 and A96 exhibit significantly lower enthapies ($\Delta V_{tot} = -33$ and −22 kJ/mol) which is compensated by a larger entropic contribution of 26 and 22 kJ/mol, respectively. Although this comparison highlights certain aspects of the force fields, it should be kept in mind that the partition in solute and solvent contributions is not physical in many cases (e.g., the entropy is not additive). Furthermore, there may be a quite large uncertainty in the calculation of the entropy of short-lived conformational states, such as α_R in the case of trialanine.

3.3. Conformational Dynamics. The potentials of mean force discussed above point out the possibility of conformational transitions between the various stable conformers of trialanine. The potential in ϕ mainly reflects transitions between the two extended conformers β and P_{II}. Because of the small barrier between these conformations and due to their similarity, these transitions are quite frequent with an average lifetime of the conformers of about 10 ps. The transitions between the helix conformation α_R and the extended conformations β and P_{II}, on the other hand, require a relatively large structural rearrange-

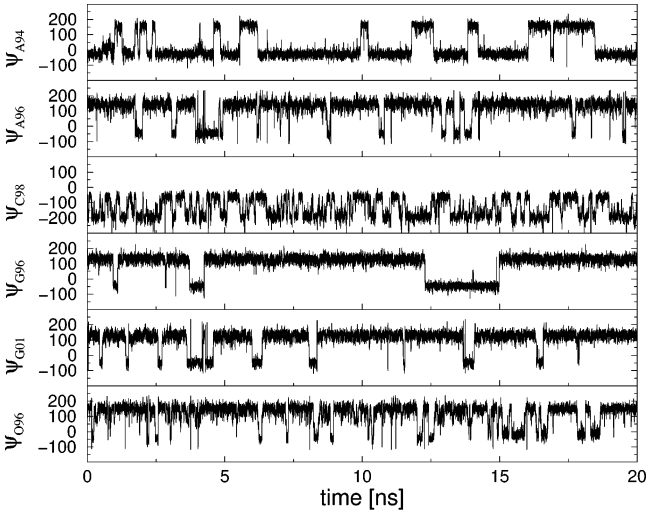

Figure 3. Time evolution of the central dihedral angle ψ of trialanine obtained for various force fields.

TABLE 4: Characterization of the Dynamical Transitions of Trialanine between the Helical (α_R) and Extended (β, P_{II}) Conformations[a]

model	N_t	τ_α [ps]	$\tau_{\beta P_{II}}$ [ps]	$\Delta G^{\#}_{\alpha}$	$\Delta G^{\#}_{\beta P_{II}}$	τ_0 [ps]	$\psi^{\#}$ [deg]
A94	40	712	258	10.7	7.4	10.5	83.4
A96	62	77	640	7.7	11.2	6.6	21.5
C98	261	74	81	4.0	4.2	14.9	−136.8
G96	14	487	1344	13.1	16.2	2.4	11.0
G01	41	225	530	12.0	14.1	1.8	21.0
O96	54	69	507	6.7	12.4	3.4	6.2

[a] Shown are the number of transitions N_t within the simulation time of 20 ns, the average lifetimes τ_α and $\tau_{\beta P_{II}}$ of the conformers, the barrier-free transition time τ_0, as well as the free-energy differences $\Delta G^{\#}_{\alpha}$ and $\Delta G^{\#}_{\beta P_{II}}$ (in kJ/mol) between the conformers and the barrier located at $\psi^{\#}$.

ment. This results in a larger barrier, which turns out to be quite sensitive to the force field used. In the following, we focus on the latter transitions which can be monitored by the central dihedral angle ψ.

To illustrate the dynamics of these transitions, Figure 3 shows the time evolution of $\psi(t)$ as obtained for the various force fields. Although the actual transition event typically lasts between 1 and 10 ps in all cases, the frequency of the transitions and thus the lifetimes of the conformers are seen to depend significantly on the force field used. Table 4 summarizes these finding by listing the number of transitions N_t within the simulation time of 20 ns as well as the average lifetimes τ_α and $\tau_{\beta P_{II}}$ of the helix and the extended conformations, respectively. Interestingly, we find about an order of magnitude difference between the slowest or most rigid model G96 (14 transitions) and the fastest or most flexible model C98 (260 transitions).

Table 4 also lists the free-energy differences $\Delta G^{\#}_{\alpha}$ and $\Delta G^{\#}_{\beta P_{II}}$ between the barrier (denoted by #) and the helical and extended conformations, respectively. Assuming a simple Arrhenius-type process, i.e., $\tau_i = \tau_{0_i} \exp(\Delta G^{\#}_i/k_B T)$ ($i = \alpha, \beta/P_{II}$), the lifetimes τ_α and τ_β are directly connected to the free-energy differences $\Delta G^{\#}_{\alpha}$ and $\Delta G^{\#}_{\beta P_{II}}$ between the barrier (denoted by #) and the helical and extended conformations, respectively. From this analysis, barrierless transition times $\tau_0 = \tau_{0\alpha} \approx \tau_{0\beta P_{II}}$ between 2 and 15 ps are found. Furthermore, it is seen that the location of the barrier $\psi^{\#}$ depends largely on the force field used. Although $\psi^{\#} \approx 10-20°$ for A96, G96, G01, and O96, a quite larger value of 83° is found for A94. In the case of C98, we obtain $\psi^{\#} = -137°$, indicating that it is energetically more favorable to make the transition in the other direction of ψ.

3.4. Comparison to Experiment. *3.4.1. 2D-IR Spectroscopy.* The 2D-IR studies of Woutersen and Hamm[11−13] as well as the polarized visible Raman and FTIR experiments of Schweitzer-Stenner and co-workers[36,37] have been discussed on the basis of a simple exciton model, which describes the amide I vibrational band in a local site basis[9,59]

$$H = \begin{pmatrix} \epsilon_1 + \delta\epsilon_1(t) & J + \delta J(t) \\ J + \delta J(t) & \epsilon_2 + \delta\epsilon_2(t) \end{pmatrix} \tag{10}$$

where $\delta\epsilon_1(t)$, $\delta\epsilon_2(t)$, and $\delta J(t)$ are instantaneous deviations of the site energies and the intersite couplings from their time-average values ϵ_1, ϵ_2, and J. Diagonalizing this Hamiltonian with respect to its time average, we obtain the eigenstates of the system with energies ω_1 and ω_2. These vibrational frequencies can be measured in a standard IR experiment, whereas the coupling J can be extracted from the cross-peak intensities in the 2D-IR spectrum, similar as in the case of 2D-NMR. Being mainly caused by the electrostatic interaction between the transition dipoles whose orientation depends on the ϕ,ψ dihedral angles of the peptides groups, this coupling directly monitors the structure of the peptide backbone. By using femtosecond IR laser pulses, moreover, the delay time between the pulses can be employed to monitor the fluctuations $\delta\epsilon(t)$ and $\delta J(t)$, which reflect the conformational dynamics of the system.

Based on the exciton model described above, Woutersen and Hamm performed a global fit of the calculated 2D-IR spectra to the experimental data. They obtained for the intersite coupling $J = 6$ cm^{-1} and for the angle between the two transition dipole vectors $\theta = 106°$.[11] Similar values ($J = 4$ cm^{-1}, $\theta = 119°$) were obtained by Schweitzer-Stenner and co-workers using polarized visible Raman and FTIR spectroscopy.[36] Employing ab initio calculations of Torii and Tasumi who computed the vibrational coupling J as a function of the two dihedral angles ϕ and ψ,[39] both groups concluded that trialanine is mainly found in the P_{II} conformation at $(\phi,\psi) = (-60°, +140°)$[11] and $(\phi,\psi) = (-66°, +140°)$,[36] respectively. This result is somewhat in variance with a very recent study of Schweitzer-Stenner, who tried to avoid the usage of ab initio data by additionally measuring the orientational angle between the two peptide groups, $\theta_P = 124°$.[37] This analysis yielded the peptide geometry $(\phi,\psi) = (-126°, +178°)$, which corresponds to the extended β conformation.

To compare these experimental data to our MD studies, we have calculated the mean value of the angles θ and θ_P directly from the geometries obtained from the trajectories[60] and determined the mean vibrational coupling J by using the ab initio-based map $J(\phi,\psi)$ of Torii and Tasumi.[39] Table 5 comprises all available experimental and calculated results, where the latter data are given state-resolved (i.e., calculated for a specific conformation β, P_{II}, or α) and as average over the population-weighted conformational states.

Considering θ, the angle between the two transition dipole vectors, the experimental result of $\theta \approx 110°$ seems to indicate that trialanine predominantly exists in the P_{II} conformation, because the MD calculations for this conformer are found to result in a similar value for θ. Similarly, the experimental mean value of the coupling $J \approx 5$ cm^{-1} points toward the P_{II} conformation of the peptide. It should be noted, however, that these conclusions only hold within the assumption that trialanine occupies only a *single* conformational state. Allowing for a multistate model, it is found that both experimental values are quite well reproduced by the force fields A96, G96, G01, and

TABLE 5: Comparison of Experimental and Calculated Results Obtained for Trialanine in Water

model	state	P [%]	θ [deg]	J [cm^{-1}]	θ_P [deg]	δJ^2 [cm^{-2}]	Δ_0^2 [cm^{-2}]	$^3J_1$ [Hz]	$^3J_2$ [Hz]
A94	β	3	128.2	3.5	139.0	4.0	3.0	9.56	5.52
	P_{II}	13	104.1	8.4	83.5	34.3	1.1	4.76	5.14
	α_R	80	68.6	7.2	90.0	20.2	8.4	5.78	5.59
	all		78.1	7.0	92.8	20.8	13.6	5.86	5.53
A96	β	44	130.5	3.8	132.4	4.6	4.2	8.90	7.30
	P_{II}	41	113.6	4.8	87.0	33.3	1.7	5.10	7.30
	α_R	14	54.3	10.1	80.5	28.1	14.0	6.11	7.00
	all		111.3	5.2	106.8	19.6	29.1	7.03	7.23
C98	β/P_{II}	55	106.4	6.1	97.6	18.7	4.2	8.12	6.62
	α_R	45	33.4	14.3	76.0	16.0	5.9	7.79	6.66
	all		71.9	10.0	87.4	17.5	30.6	7.98	6.64
G96	β	42	140.5	3.1	121.9	1.8	1.4	10.26	7.17
	P_{II}	41	116.9	3.5	91.2	30.2	1.9	5.02	7.28
	α_R	16	53.5	10.5	87.3	18.4	2.5	5.81	8.13
	all		117.7	4.2	103.8	16.1	16.5	7.31	7.19
G01	β	41	141.8	3.0	120.4	2.1	2.2	10.04	7.54
	P_{II}	34	122.4	2.4	91.9	37.7	1.4	5.28	7.37
	α_R	22	49.2	11.2	83.7	20.7	4.5	6.16	7.68
	all		111.6	5.2	102.6	18.1	20.7	7.30	7.46
O96	β/P_{II}	88	122.0	3.5	107.1	14.4	6.3	8.30	7.12
	α_R	12	52.6	10.1	77.6	23.4	12.7	7.48	7.97
	all		117.3	4.1	105.0	15.4	16.2	8.24	7.18
exp.			106[a]	6.0[a]		27.0[b]	25.0[c]	5.27[c]	6.22[c]
			119[e]	4.0[e]	124[e,f]			5.17[d]	6.19[d]

[a] From ref 11. [b] From ref 12. [c] From ref 35. [d] From ref 34. [e] From ref 36. [f] From ref 37.

O96, which all predict the population ratio of the conformers as $P_\beta/P_{PII}/P_\alpha \approx 40/40/15$. On the other hand, the state-averaged results for the other two models, A94 and C98, do not match the experimental data.

As mentioned above, the experimental result for the orientational angle between the two peptide groups, $\theta_P = 124°$, is somewhat in variance with the interpretation of the other IR data. In agreement with the experimental interpretation in ref 37, the MD studies clearly show that this value of θ_P indicates a preference for the β conformation. In this case, however, the experimental value cannot be reproduced by any of the state-averaged MD results.

To better understand the effects of the conformational average, it is instructive to consider the probability distributions of θ as determined from the MD simulations. Figure 4 shows the state-averaged distribution as obtained for the various force fields and, for the representative example of the force field A96, its state-resolved contributions. The different positions and populations of the conformers obtained for the various force fields is directly reflected in their θ distribution. Consequently, all but the A94 force field yield a bimodal distribution, with the two peaks corresponding to the helical α_R and the extended β, P_{II} conformations. Analogous studies performed for the distribution of the vibrational coupling J yielded similar results.

To summarize, the force fields A96, G96, G01, and O96 are able to reproduce the experimental IR data; however, the comparison leaves open the question, whether the peptide occurs exclusively in the P_{II} conformation or whether it exists as a superposition of the three conformational states β, P_{II}, and α_R.

3.4.2. NMR Spectroscopy. Homonuclear $^3J(H^N-H^\alpha)$ couplings of trialanine in D_2O at pD = 1 have been measured,[34,35] yielding $^3J_1 \equiv {}^3J(\phi)$ reflecting the central backbone dihedral angle ϕ and $^3J_2 \equiv {}^3J(\phi_c)$ reflecting the backbone dihedral angle ϕ_C of the carbonyl terminal. Employing the Karplus relation[61]

$$^3J(\phi) = A\cos^2(\phi + \phi_0) + B\cos(\phi + \phi_0) + C \quad (11)$$

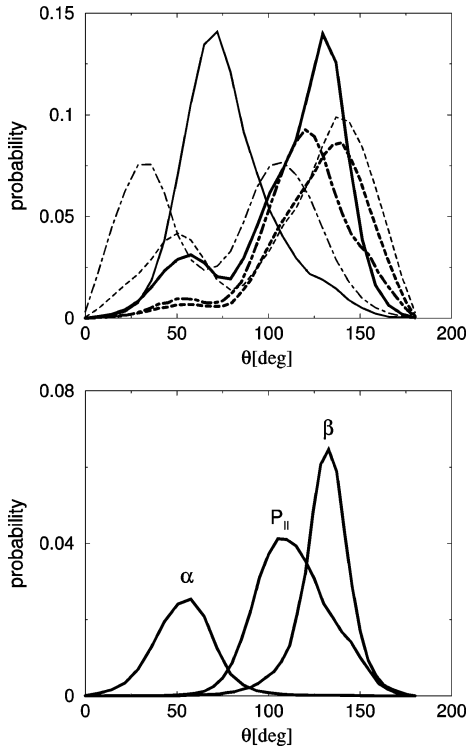

Figure 4. Probability distribution of the angle θ between the amide I transition−dipole vectors of trialanine. The upper panel shows the comparison of the force fields A94 (thin solid lines), A96 (thick solid lines), C98 (thin dotted-dashed lines), G96 (thick dashed lines), G01 (thin dashed lines), and O96 (thick dotted-dashed lines). The lower panel displays the contributions of the three conformational state α, P_{II}, and β to the distribution obtained for A96.

with H^N-H^α parameters $\phi_0 = -60°$, $A = 9.5$ Hz, $B = -1.4$ Hz, and $C = 0.3$ Hz,[62] we have calculated both ^3J coupling constants directly from the MD simulations. Table 5 compares the state-resolved computational results for $^3J_1$ to its experimental value of ≈ 5.2 Hz. Assuming a single conformational state of trialanine is occupied, the force fields A94, A96, G96, and G01 clearly predict the P_{II} conformation. The $^3J_1$ coupling calculated for the P_{II}-like state of the C98 and O96 force fields, on the other hand, is significantly too large. This is because these models exhibit only a single extended conformation which is located between the usual P_{II} and β state (see Figure 1).

Most interesting is the fact, however, that for all force fields the β and the α_R conformers yield a too large value of $^3J_1$; that is, we find $^3J_1 = 9$ Hz for β and $^3J_1 = 6$ Hz for α_R. From this finding, one can (i) out-rule a significant (i.e., larger than 5−10%) population of the extended β conformation and (ii) predict that the helical α_R conformer can be only little occupied (i.e., $\lesssim$20%). Compared to the other experimental observables, the $^3J_1$ therefore represents the clearest indication for the structure of trialanine.

As is expected, the results for the $^3J_2$ coupling monitoring the dihedral angle ϕ_C of the C-terminal backbone depends only little on the (ϕ,ψ) conformation of the peptide. A closer analysis shows that the distribution in ϕ_C typically exhibits two peaks at $\phi_C \approx -130°$ (the β^C state) and at $\phi_C \approx -70°$ (the $P_{II}C$ state), which give rise to a $^3J_2$ coupling of 9 and 5 Hz, respectively. The deviation of the calculated and experimental values of $^3J_2$ indicate that the simulations overestimate the population of the β^C conformer.

3.4.3. Time-Resolved 2D-IR Spectroscopy. Introducing the delay time between the two laser pulses as a third variable, the time- and frequency-resolved IR experiments also allow us to

obtain information on the conformational dynamics of the solvated peptide. By measuring the vibrational cross-relaxation rates between the two amide I modes of trialanine, Woutersen et al. obtained an estimate of the cross-relaxation correlation function of the system,[12] which can be fitted to the biexponential function

$$\langle \delta J(t) \delta J^2(0) \rangle = \delta J^2 (w_1 e^{-t/\tau_1} + w_2 e^{-t/\tau_2}), \qquad (12)$$

where $\delta J^2 = \langle \delta J^2(0) \rangle$ denotes the squared amplitude of the fluctuations and τ_1, τ_2 are the correlation times with the weights w_1, w_2 ($w_1 + w_2 = 1$). The short correlation time $\tau_1 \approx 100$ fs accounts for the inertial motion of the peptide, whereas the larger correlation time $\tau_2 \approx 2$ ps reflects its diffusional motion. For all conformers and force fields under consideration, the calculated correlation times turned out to be quite similar to the experimental data. However, the overall amplitude of the fluctuations δJ^2 was found to depend significantly on the conformational state and the force field used.

Table 5 compares the magnitude of the fluctuations δJ^2 as obtained for the various conformations and force fields. The comparison demonstrates that most of the fluctuations are sampled in the P_{II} and the α state, whereas the β conformation hardly contributes to δJ^2, because the $J(\phi,\psi)$ map is quite flat in this region. Given that the experimentally measured value for the δJ^2 is quite large, these findings again suggest that trialanine predominantly occupies the P_{II} state and, to a smaller extent, also the α state. It should be kept in mind, however, that these results rely on the ab initio-based map $J(\phi,\psi)$ of Torii and Tasumi.[39] As only fluctuations in the dihedral angles ϕ and ψ are considered by this map, the calculations can only be expected to yield a lower bound of δJ^2. In reality, other degrees of freedom are also expected to contribute to the fluctuations δJ^2.

In a very recent paper, it was demonstrated that time-resolved 2D-IR spectroscopy also allows us to characterize the frequency fluctuations $\delta\omega_{01}(t) = \omega_{01}(t) - \langle \omega_{01} \rangle$ of the $v = 0 \rightarrow 1$ amide I transition of trialanine.[35] Employing Kubo's line-shape theory for the modeling of the spectra, the frequency fluctuation correlation function $\langle \delta\omega_{01}(t) \delta\omega_{01}(0) \rangle$ of trialanine and *N*-methyl-acetamide, a commonly used model system with a single peptide bond, was determined. Interestingly, it was found that, in contrast to *N*-methyl-acetamide, the amide I band of trialanine exhibits a significant inhomogeneous broadening for times $\gtrsim 4$ ps. That is, the frequency fluctuation correlation function assumes a constant value Δ_0^2 at times that are large on the experimental time scale.

To calculate the frequency fluctuation correlation function $\langle \delta\omega_{01}(t) \delta\omega_{01}(0) \rangle$ directly from the MD simulations, we have performed extensive DFT calculations on the B3LYP/6-31+G(d) level of theory.[38] This yielded a two-dimensional frequency map $\omega(\phi,\psi)$ of the two amide I modes of trialanine, which was used to calculate the inhomogeneous broadening Δ_0^2. Table 5 compares the experimental result $\Delta_0^2 = 25$ cm^{-2} to the calculated data obtained for the various conformations and force fields. The magnitude of the fluctuations is seen to depend significantly on the conformational state, whereby the smallest values of $\Delta_0 \approx 1-2$ cm^{-2} are obtained for the P_{II} state, followed by the β state with $\approx 2-4$ cm^{-2} and the α_R state with $\approx 3-14$ cm^{-2}. Interestingly, it is seen that in all cases the frequency fluctuations averaged over the complete trajectory are much larger than the fluctuations in a specific conformational state. This finding clearly shows that the large inhomogeneity is caused by conformational (ϕ,ψ) transitions of trialanine, which are absent in *N*-methyl-acetamide. A closer analysis of the data reveals that particularly the $\alpha_R \leftrightarrow P_{II}$ transitions are responsible for the inhomogeneous broadening.[35]

The combined experimental/computational investigations provide a direct clue on the existence of conformational transitions of a small peptide such as trialanine. Combined with the results of the NMR studies reported above, one may conclude that trialanine in aqueous solution populates predominantly ($\gtrsim$80%) the P_{II} state, to a smaller amount ($\lesssim$20%) the α_R state, and only insignificantly ($\lesssim$5−10%) the extended β state.

Discussion and Conclusions

Adopting trialanine as a paradigm of a small peptide in aqueous solution, we have presented a comprehensive comparison of six popular force fields, including the recent versions of the AMBER, CHARMM, GROMOS, and OPLS models. For all force fields under consideration, we have performed 20 ns long MD simulations to study in detail the structure and conformational dynamics of the solvated peptide. When high-level (B3LYP/6-31+G(d)) DFT calculations are employed, a number of observable quantities have been calculated directly from the MD data and compared to experiment. Based on these studies, it has been concluded that trialanine populates predominantly ($\gtrsim$80%) the P_{II} state, to a smaller amount ($\lesssim$20%) the α_R state, and only insignificantly ($\lesssim$5%) the extended β state.

To characterize the stable conformers of trialanine in water, we have considered the population probabilities (Figure 1 and Table 2) and the corresponding free-energy profiles (Figure 2 and Table 4) along the central dihedral angles (ϕ,ψ) of the peptide. The simulations have shown that, in a similar way, the force fields AMBER A96, GROMOS G96 and G01, and OPLS O96 predict that solvated trialanine is found to equal parts in the extended conformations β ($\approx$40%) and P_{II} ($\approx$40%) and to a smaller part ($\approx$20%) in the helix conformation α_R. Although the overall ratio of extended and helical populations is in agreement with experimental evidence, these force fields thus clearly oversample the β conformation. On the other hand, the AMBER A94 and the CHARMM C98 force fields predict a relatively large population of the helical α_R conformation, whereas the β conformer is hardly populated. Here the latter result is in accordance to experiment, but the α_R state is clearly oversampled relative to the P_{II} state.

It is interesting to compare these findings to the results obtained for *isolated* trialanine. As discussed in section 3.1, the force fields A96, G96, G01, and O96 clearly favor the β state over the α_R states. This is exactly the group of models that also over-samples the β conformation in solution. On the other hand, the force fields A94 and C98 favor the α_R state over the β state in the gas phase. This group of models is the one that also oversamples the α_R conformation in solution. Seen from this angle, it appears that the performance of the force fields in solution depends strongly on their properties in the gas phase.

The example of the two AMBER force fields A94 and A96 has demonstrated that already minor modifications of the force field may significantly change the population ratio of the conformational states. In this case, the A96 model was derived from the A94 model through a reparametrization of the backbone dihedral parameters, which were adjusted to reproduce the gas-phase energy difference between extended β and constrained α_R helical conformations for the alanine tetrapeptide, as calculated by high-level ab initio methods.[42,64] The two GROMOS force fields G96 and G01, on the other hand, differ

in their parametrization of the aliphatic carbons,[45] which was found to have only minor effects on the population of the conformational states of trialanine.

The discussion again reflects the fact that the outcome of biomolecular simulations typically depends on free-energy differences of less than $k_BT = 2.5$ kJ/mol. Clearly, such an accuracy is hard to achieve by an empirical force field. As a remedy, one could augment the microscopic MD description with the correct statistical weights obtained from experiment. For the AMBER and GROMOS force fields, this amounts to discarding the β conformation and restricting the analysis to the P_{II} state (with a weight of $\gtrsim$80%) and the α_R state (with a weight of $\lesssim$20%). When this is done, virtually all available experimental data can be reproduced with high accuracy. This strategy cannot be applied to the CHARMM and the OPLS force fields, however, because these models exhibit only a single peak for both extended conformations.

Employing a combined MD/quantum-chemical approach, we have calculated a number of experimentally observable quantities. The study included the following: (i) Geometric properties of the molecule such as the angles θ and θ_P, which can directly be calculated from the MD trajectory. (ii) Properties of the amide I exciton system such as the intersite coupling J and its fluctuation δJ^2. In addition to the MD data, the evaluation of these quantities required quantum-chemical studies. (iii) NMR properties such as the $^3J(H^N-H^\alpha)$ couplings of the peptide, which can be calculated from the MD data by using a Karplus-type relation. Although the theoretical level may be modest, the investigations nevertheless represent a *first principles* description of the experiment, in the sense that no free parameters or experimental data are included.

In the case of trialanine, two experimental observables proved to be particularly valuable. First, the $^3J(H^N-H^\alpha)$ coupling reflecting the central backbone dihedral angle ϕ was found to reflect quite sensitively the conformational states of the peptide. Because the experimental value of ^3J happened to be a lower bound of the calculated data, the comparison of theory and experiment helped to out-rule the population of the β conformational state. Second, the experimentally measured large inhomogeneous broadening Δ_0 of the amide I band of trialanine turned out to be a key observation. Here our studies suggested that $\alpha_R \leftrightarrow P_{II}$ conformational transitions are the origin of this inhomogeneity. This shows that trialanine in water occurs in at least two different conformations.

Recently, we have extended our studies by MD simulations using the new version of the OPLS force field[19] combined with the TIP5P water model.[65] Although the overall performance is similar to the previous version O96, the new parametrization represents a clear improvment in the sense that the population probabilities are now 12% for the β, 65% for the P_{II}, and 18% for the α conformation, respectively, that is, very close to the experimental findings (see the Supporting Information). The crucial NMR $^3J_1$ coupling, however, still came out somewhat too large compared to the experiment (7.1 Hz for the conformational average). We also wish to mention the very recent work of Hermans and co-workers, who studied the alanine and glycine dipeptides comparing several standard force fields and a semiempirical QM/MM description.[40] These authors found that the distribution from the QM/MM simulation shows greater similarity with the distribution in high-resolution protein structures than is the case for any of the standard force fields.

Although all force fields considered provided a relatively coherent picture of the structure of trialanine, our investigations showed that the various models differ considerably in the description of the dynamical properties of the system. Considering the $\alpha_R \leftrightarrow P_{II}$ conformational transitions, for example, it was found that the lifetimes of the conformational states differ by more than an order of magnitude, depending on which model was used. At the present time, it is therefore not clear to what extent commonly used force fields are capable of correctly describing *nonequilibrium* dynamics such as the folding or unfolding of a peptide. Time-resolved picosecond spectroscopy of photoinduced folding processes of small peptides,[66] in combination with a first principles modeling of the experiment as described above, therefore holds a great promise to improve our understanding of peptide conformational dynamics in atomic detail.

Acknowledgment. We thank Peter Hamm, Rainer Hegger, Reinhard Schweitzer-Stenner, and Christian Griesinger for many inspiring and illuminating discussions. Financial support by the Deutsche Forschungsgemeinschaft and the Fonds der Chemischen Industrie is gratefully acknowledged.

Supporting Information Available: Results of additional test calculations to assure the significance and convergence of our studies. This material is available free of charge via the Internet at http://pubs.acs.org.

References and Notes

(1) Allen, M. P.; Tildesley, D. J. *Computer Simulation of Liquids;* Oxford University: New York, 1987.
(2) McCammon, J. A.; Harvey, S. C. *Dynamics of Proteins and Nucleic Acids*; Cambridge University Press: New York, 1987.
(3) Leach, A. R. *Molecular Modeling*; Pearson Education Limited: London, 1996.
(4) Karplus, M. J.; Petsko, G. A. *Nature (London)* **1990**, *347*, 631.
(5) van Gunsteren, W. F.; Berendsen, H. J. C. *Angew. Chem., Int. Ed. Engl.* **1990**, *29*, 992.
(6) Kollman, P. A. *Chem. Rev.* **1993**, *93*, 2395.
(7) Brooks, C. L., III.; Case, D. A. *Chem. Rev.* **1993**, *93*, 2487.
(8) Mukamel, S., Hochstrasser, R. M., Eds. Special Issue on Multidimensional Spectroscopies. *Chem. Phys.* **2001**, *266*, Nos. 2−3.
(9) Hamm, P.; Lim, M.; Hochstrasser, R. M. *J. Phys. Chem. B* **1998**, *102*, 6123.
(10) Zanni, M. T.; Ge, N.-H.; Kim, Y. S.; Hochstrasser, R. M. *Proc. Natl. Acad. Sci. U.S.A.* **2001**, *98*, 11265.
(11) Woutersen, S.; Hamm, P. *J. Phys. Chem. B* **2000**, *104*, 11316.
(12) Woutersen, S.; Hamm, P. *J. Chem. Phys.* **2001**, *114*, 2727.
(13) Woutersen, S.; Mu, Y.; Stock, G.; Hamm, P. *Proc. Natl. Acad. Sci. U.S.A.* **2001**, *98*, 11254.
(14) Scheurer, C.; Mukamel, S. *J. Chem. Phys.* **2001**, *115*, 4989−5004.
(15) Head-Gordon, T.; Head-Gordon, M.; Frisch, M. J.; Brooks, C. L., III; Pople, J. A. *J. Am. Chem. Soc.* **1991**, *113*, 5989.
(16) Cornell, W. D.; Gould, I. R.; Kollman, P. *J. Mol. Struct.* **1997**, *392*, 101.
(17) Beachy, M. D.; Chasman, D.; Murphy, R. B.; Halgren, T. A.; Friesner, R. A. *J. Am. Chem. Soc.* **1997**, *119*, 5908.
(18) Han, W.-G.; Jalkanen, K. J.; Elstner, M.; Suhai, S. *J. Phys. Chem. B* **1998**, *102*, 2587.
(19) Kaminski, G. A.; Friesner, R. A.; Tirado-Rives, J.; Jorgensen, W. L. *J. Phys. Chem. B* **2001**, *105*, 6474.
(20) Friesner, R. A.; Dunietz, B. D. *Acc. Chem. Res* **2001**, *34*, 351.
(21) Wei, D.; Guo, H.; Salahub, D. R. *Phys. Rev. E* **2001**, *64*, 011907.
(22) Pettitt, B. M.; Karplus, M. J. *J. Phys. Chem.* **1988**, *92*, 3994.
(23) Tobias, D. J.; Brooks, C. L., III. *J. Phys. Chem.* **1992**, *96*, 3864.
(24) Samuelson, S.; Tobias, D. J.; Martyna, G. J. *J. Phys. Chem. B* **1997**, *101*, 7592.
(25) Samuelson, S.; Martyna, G. J. *J. Phys. Chem. B* **1999**, *103*, 1752.
(26) Blatt, H. D.; Smith, P. E.; Pettitt, B. M. *J. Phys. Chem. B* **1997**, *101*, 7628.
(27) Apostolakis, J.; Ferrara, P.; Calfish, A. *J. Chem. Phys.* **1999**, *110*, 2099.
(28) Smith, P. E. *J. Chem. Phys.* **1999**, *111*, 5568.
(29) Kalko, S. G.; Guiàrdia, E.; Padró, J. A. *J. Phys. Chem. B* **1999**, *103*, 3935.
(30) Park, C.; Carlson, M. J.; Goddard, W. A. *J. Phys. Chem. A* **2000**, *104*, 2498.
(31) Mu, Y.; Stock, G. *J. Phys. Chem. B* **2002**, *106*, 5294.

(32) Hu, H.; Elstner, M.; Hermans, J. *Proteins* **2002**, in press.
(33) Poon, C.-D.; Samulski, E. T. *J. Am. Chem. Soc.* **2000**, *122*, 5642.
(34) Dorai, K.; Griesinger, C. to be published.
(35) Woutersen, S.; Pfister, R.; Hamm, P.; Mu, Y.; Kosov, D.; Stock, G. *J. Chem. Phys.* **2002**, *117*, 6833.
(36) Schweitzer-Stenner, R.; Eker, F.; Huang, Q.; Griebenow, K. *J. Am. Chem. Soc.* **2001**, *123*, 9628.
(37) Schweitzer-Stenner, R. *Biophys. J.* **2002**, *83*, 523.
(38) Kosov, D. S.; Mu, Y.; Stock, G. to be published.
(39) Torii, H.; Tasumi, M. *J. Raman Spectrosc.* **1998**, *29*, 81.
(40) Although a few authors have compared specific aspects of force fields (see, e.g., refs 24 and 28), the only other systematic and comprehensive comparison we know of is the very recent work of Hermans and co-workers [ref 32].
(41) Cornell, W. D.; Cieplak, P.; Bayly, C. I.; Gould, I. R.; Merz, K. M., Jr.; Ferguson, D. M.; Spellmeyer, D. C.; Fox, T.; Caldwell, J. W.; Kollman, P. A. *J. Am. Chem. Soc.* **1995**, *117*, 5179.
(42) Kollman, P.; Dixon, R.; Cornell, W.; Fox, T.; Chipot, C.; Pohorille, A. In *Computer Simulation of Biomolecular System 3*; van Gunsteren, W. F., Weiner, P. K., Wilkinson, A. J. Eds.; Kluwer Academic: Dordrecht, The Netherlands, 1997; p 83.
(43) MacKerell, A. D., Jr.; Bashford, D.; Bellott, M.; Dunbrack, R. L., Jr.; Evanseck, J. D.; Field, M. J.; Fischer, S.; Gao, J.; Guo, H.; Ha, S.; Joseph-McCarthy, D.; Kuchnir, L.; Kuczera, K.; Lau, F. T. K.; Mattos, C.; Michnick, S.; Ngo, T.; Nguyen, D. T.; Prodhom, B.; Reiher, W. E., III.; Roux, B.; Schlenkrich, M.; Smith, J. C.; Stote, R.; Straub, J.; Watanabe, M.; Wiorkiewicz-Kuczera, J.; Yin, D.; Karplus, M. *J. Phys. Chem. B* **1998**, *102*, 3586.
(44) Van Gunsteren, W. F.; Billeter, S. R.; Eising, A. A.; Hünenberger, P. H.; Krüger, P.; Mark, A. E.; Scott, W. R. P.; Tironi, I. G. *Biomolecular Simulation: The GROMOS96 Manual and User Guide*; Vdf Hochschulverlag AG an der ETH Zürich: Zürich, 1996.
(45) Schuler, L. D.; Daura, X.; van Gunsteren, W. F. *J. Comput. Chem.* **2001**, *22*, 1205.
(46) Jorgensen, W. L.; Maxwell, D. S.; Tirado-Rives, J. *J. Am. Chem. Soc.* **1996**, *118*, 11225.
(47) Hünenberger, P. H.; van Gunsteren, W. F. In *Computer Simulation of Biomolecular System 3*; van Gunsteren, W. F., Weiner, P. K., Wilkinson, A. J., Eds.; Kluwer Academic: Dordrecht, The Netherlands, 1997; p 3.
(48) Case, D. A.; Pearlman, D. A.; Caldwell, J. W.; Cheatham, T. E., III.; Ross, W. S.; Simmerling, C. L.; Darden, T. A.; Merz, K. M.; Stanton, R. V.; Cheng, A. L.; Vincent, J. J.; Crowley, M.; Tsui, V.; Radmer, R. J.; Duan, Y.; Pitera, J.; Massova, I.; Seibel, G. L.; Singh, U. C.; Weiner, P. K.; Kollman, P. A. *Amber6*; University of California: San Francisco, CA, 1999.
(49) Tirado-Rives, J.; Jorgensen, W. L. *Biochemistry* **1991**, *30*, 3864.
(50) Ryckaert, J. P.; Cicotti, G.; Berendsen, H. J. C. *J. Comput. Phys.* **1977**, *23*, 327.
(51) Berendsen, H. J. C.; Postma, J. P. M.; van Gunsteren, W. F.; Dinola, A.; Haak, J. R. *J. Chem. Phys.* **1984**, *81*, 3684.
(52) Berendsen, H. J. C.; Postma, J. P. M.; van Gunsteren, W. F.; Hermans, J. In *Intermolecular Forces*; Pullman, B., Ed.; Reidel: Dordrecht, The Netherlands 1981; p 331.
(53) In the case of GROMOS96 force field, the good agreement of the free-energy profiles were shown in ref 31. Moreover, this paper presents 20 ns MD simulations at $T = 350$ K.
(54) Amadei, A.; Linssen, A. B.; Berendsen, H. J. *Proteins* **1993**, *17*, 412.
(55) Andricioaei, I.; Karplus, M. *J. Chem. Phys.* **2001**, *115*, 6289.
(56) Frisch, M. J.; Trucks, G. W.; Schlegel, H. B.; Scuseria, G. E.; Robb, M. A.; Cheeseman, J. R.; Zakrzewski, V. G.; Montgomery, J. A., Jr.; Stratmann, R. E.; Burant, J. C.; Dapprich, S.; Millam, J. M.; Daniels, A. D.; Kudin, K. N.; Strain, M. C.; Farkas, O.; Tomasi, J.; Barone, V.; Cossi, M.; Cammi, R.; Mennucci, B.; Pomelli, C.; Adamo, C.; Clifford, S.; Ochterski, J.; Petersson, G. A.; Ayala, P. Y.; Cui, Q.; Morokuma, K.; Malick, D. K.; Rabuck, A. D.; Raghavachari, K.; Foresman, J. B.; Cioslowski, J.; Ortiz, J. V.; Stefanov, B. B.; Liu, G.; Liashenko, A.; Piskorz, P.; Komaromi, I.; Gomperts, R.; Martin, R. L.; Fox, D. J.; Keith, T.; Al-Laham, M. A.; Peng, C. Y.; Nanayakkara, A.; Gonzalez, C.; Challacombe, M.; Gill, P. M. W.; Johnson, B. G.; Chen, W.; Wong, M. W.; Andres, J. L.; Head-Gordon, M.; Replogle, E. S.; Pople, J. A. *Gaussian 98*; Gaussian, Inc.: Pittsburgh, PA, 1998.
(57) For high-level ab initio descriptions of small peptides see, for example, refs 17−20.
(58) GROMOS96 also offers a special force field (termed *43B1*) for gas-phase simulation which, however, was not used in this study for consistency reasons.
(59) Torii, H.; Tasumi, M. *J. Chem. Phys.* **1992**, *96*, 3379.
(60) Krimm, S.; Abe, Y. *Proc. Natl. Acad. Sci. U.S.A.* **1972**, *69*, 2788.
(61) Karplus, M. J. *J. Chem. Phys.* **1959**, *30*, 11.
(62) As discussed in ref 63, these "zero motion" parameters should be used when the ^3J couplings are calculated by averaging over the ^3J couplings obtained from a MD trajectory. It is noted, however, that the usage of other Karplus parameters discussed in ref 63 did not change significantly the MD-averaged results shown in Table 5.
(63) Case, D. A.; Scheurer, C.; Brüschweiler, R. *J. Am. Chem. Soc.* **2000**, *122*, 10390.
(64) Ono, S.; Nakajima, N.; Higo, J.; Nakamura, H. *J. Comput. Chem.* **2000**, *21*, 748.
(65) Mahoney, M. W.; Jorgensen, W. *J. Chem. Phys.* **2000**, *112*, 8910.
(66) Spörlein, S.; Carstens, H.; Renner, C.; Behrendt, R.; Moroder, L.; Tavan, P.; Zinth, W.; Wachtveitl, J. *Proc. Natl. Acad. Sci. U.S.A.* **2002**, *99*, 7998.